International Journal of Pressure Vessels and Piping 125 (2015) 49–65

Contents lists available at ScienceDirect

International Journal of Pressure Vessels and Piping

journal homepage: www.elsevier.com/locate/ijpvp

Engineering approach for circumferential flaws in girth weld pipes subjected to bending load

Marcelo Paredes [a, *], Claudio Ruggieri [b]

[a] Department of Mechanical Engineering, Massachusetts Institute of Technology, 77 Massachusetts Ave., Cambridge, MA 02139, USA
[b] Department of Naval Architecture and Ocean Engineering, University of Sao Paulo, Av. Prof. Mello Moraes 2231, Sao Paulo, SP 05508-030, Brazil

ARTICLE INFO

Article history:
Received 18 May 2014
Received in revised form
9 September 2014
Accepted 16 September 2014
Available online 23 September 2014

Keywords:
Girth weld pipes
EPRI methodology
Weld strength mismatch
J integral
CTOD

ABSTRACT

The current investigation pursues extending the applicability of fully plastic solutions for *J*-integral and crack-tip opening displacement (CTOD), originally cataloged in a series of handbooks (also known as EPRI handbooks), in defective girth weld pipes subjected to bending load for a wide range of surface crack dimensions and weld strength mismatch levels. The suitability of the given set of solutions in this work is constrained by a certain number of parameters that are derived from the coupled effect of weld strength mismatch and configurational effects upon near-tip stress-strain fields in heterogeneous media. These results reveal a weak dependence of coupled effect of weld strength mismatch and weld groove size upon crack driving force, when the ratio of the mismatch between weld and base normalizing stresses is considered moderate ($\leq$1.3), whereby the proposed estimation method becomes essentially valid for failure assessment procedures and fitness-for service (FFS) evaluations.

1. Introduction

The flaw acceptance criteria for girth weld pipes are derived from the Engineering Critical Assessment (ECA) procedures. They represent a critical step into design and safety operation of piping systems, including nuclear power plants, oil and gas transmission pipelines and marine risers. However, common failures in pipeline infrastructure result primarily from crack-like surface flaws (either internal or external flaws) that often occur in the weld metal and heat affected zone (HAZ) [1–3]. A major concern in integrity assessments of circumferential flaws in field girth weld pipes is the high level of axial stress present in the crack, even if the internal pressure is relatively low. The most common loading condition comes from soil and ground movements, severe thermal gradients or exhaustive service rate, and installation-induced forces. Structural components falling into this category are deep water steel catenary risers that are installed by the reeling method. This method allows pipe welding and inspection to be conducted at onshore facilities [4,5]. Then, the welded pipe is coiled around on an onboard large reeling drum and subsequently, it is transported to the exploration area where, is unreeled, straightened, and finally it is deployed to the sea floor. While faster and more cost effective, the reeling method induces large bending loads and high tensile forces into the pipeline with potential impact on stable crack propagation of undetected flaws at girth welds. To increase the fracture resistance of the welded region many codes and current fabrication practices (see Refs. [6–8] for illustrative examples) require the use of weldments with weld metal strength higher than the base plate strength. This condition is referred to as overmatched and aims to diminish the risk of structural failure caused by an undetected weld defect. While, the large plastic deformation developed around the crack-tip is transferred from the welded region to the base metal, the fracture resistance of the component will increase because of lack of surface defects. However, while the overmatch practice has been used in many structural applications effectively, the level of mismatch between the weld metal and base plate material may affect the relationship between remotely applied loading and the crack-tip driving forces.

Fitness-for-service (FFS) assessment procedures for pipes and cylinders with circumferentially-oriented cracks subjected to large bending deformation rely heavily on the accuracy of computing the *J*-integral and the crack-tip opening displacement (CTOD) [9]. The fundamental work of Kumar et al. [10] introduces a *J* estimation procedure for selected crack geometries based on fully-plastic solutions [11], which later became widely known as the EPRI methodology. The original work was extended by Zahoor [12] to include additional geometries for circumferentially and axially cracked pipes under tensile and bending loads which, nevertheless, remain

* Corresponding author.
E-mail addresses: lmparedes53042@gmail.com, lparedes@mit.edu (M. Paredes).

http://dx.doi.org/10.1016/j.ijpvp.2014.09.003
0308-0161/

Nomenclature

a	crack depth
b	remaining crack ligament
c	circumferential crack half-length
d_n	dimensionless parameter which relates J and CTOD
h	weld groove half-width
h_1	dimensionless proportionality factor between J_p and applied loading
h_4	dimensionless proportionality factor between δ_p and applied loading
m	dimensionless constant which relates J and CTOD under small scale yielding (SSY)
n	Ramberg-Osgood strain hardening exponent
t	wall-thickness
BM	base material
CTOD	crack tip opening displacement
D_e	external pipe diameter
E', E	Young's modulus under plane strain (plane stress) condition
EPRI	Electric Power Research Institute
FFS	fitness-for-service
G_5	influence coefficient to compute the stress intensity factor
J	J-integral
J_2	second invariant of the stress deviator tensor
J_e	elastic component of J-integral
J_p	plastic component of J-integral
$\overline{J}_p$	normalized plastic component of J-integral
J_{pred}	predicted value of J-integral
J_{reel}	maximum J-value attained in the reeling simulation
K_I	stress intensity factor
LLD	load-line displacement
$\mathscr{L}$	characteristic length of the cracked component
M	applied bending moment
M_0	limit bending moment
M_y	weld strength mismatch ratio
P	generalized applied load
P_0	generalized limit load
Q_s	flaw shape parameter
R_b	bending radius
R_e	external radius of pipe
R_i	internal radius of pipe
R_m	mean radius of pipe
W	structural component width
WM	weld metal
α	dimensionless parameter of the Ramberg-Osgood model
β	angular parameter related to the circumferential surface crack geometry
δ	crack-tip opening displacement
δ_e	elastic component of crack-tip opening displacement
δ_p	plastic component of crack-tip opening displacement
$\overline{\delta}_p$	normalized plastic component of crack-tip opening displacement
Δ	load-line displacement
$\overline{\varepsilon}$	true (logarithmic) strain
ε_e	elastic strain component
ε_p	plastic strain component
ε_0	reference strain
ε_z^b	longitudinal bending strain
$\varepsilon_{z,\max}^b$	maximum value of longitudinal bending strain
ς_k	coefficients for the polynomial fitting of h factors
θ	half-angle describing the surface crack length
ν	Poisson's ratio
ρ_0	initial crack tip blunting radius
$\overline{\sigma}$	true stress
σ_b	global or net-section bending stress
σ_{uts}	ultimate tensile stress
σ_0	reference stress

limited to a few crack geometries and material (strain hardening) properties. Moreover, these crack driving force solutions do not address the effects of mechanical heterogeneity associated with weld strength mismatch on the near-tip stress and strain fields for circumferentially cracked pipes. Recent work from Chiodo and Ruggieri [13] (referred to as CR) has largely expanded the fully plastic solutions for J and CTOD in circumferentially cracked pipes subjected to pure bending load with varying crack geometries and strain hardening properties. The extensive analysis conducted in that study provides a full set of non-dimensional functions that relate the plastic components of J and CTOD with remote loading. They have also successfully applied these fully plastic solutions to predict maximum J-values attained during the reeling of pipes with varying circumferential crack geometries for X60 pipeline steel.

The focus of this article is to demonstrate the applicability of fully plastic solutions in defective welded pipes containing circumferential surface cracks under pure bending load, including various crack geometries and mismatch levels. This investigation broadens the scope of the previous work done by CR [13] which only addressed homogeneous configurations without weldments. The presentation begins with a summary of the fully-plastic solution scheme upon which J is derived for homogeneous condition (no weldments), subsequently, a proposed formulation for welded structures is presented. This is followed by the description of 3D nonlinear analysis of girth weld cracked pipes with circumferential surface flaws having different crack depth to pipe wall thickness (a/t) ratio and various crack lengths (θ/π) for a wide range of material properties, as characterized by different levels of weld strength mismatch (M_y). The 3D results provide a large set of dimensionless functions relating the elastic–plastic crack-tip driving forces, J and CTOD, with the applied (remote) bending moment which enter directly into FFS procedures of thin-walled cylindrical components.

2. Fully plastic solutions for J and CTOD in girth welds pipes with circumferential cracks

This section introduces the essential features of the theoretical framework needed to determine J and CTOD for defective girth weld pipes with circumferential cracks under bending. This engineering approach is based on fully plastic solutions for power law hardening materials incorporating the effects of weld strength mismatch. The resulting methodology follows a similar development previously presented by CR [13] for cracked bodies, in which the material is conveniently characterized by a power law hardening stress-strain behavior. We have omitted details of the fully plastic analysis and directed attention to estimation solutions applicable to pipes and cylinders having stationary (circumferential) cracks located at the girth weld centerline and subjected to monotonically increasing loading (bending moment). The procedure to estimate the J integral for a cracked component, such as a circumferentially cracked pipe, begins by considering the elastic and plastic contributions to the strain energy under Mode I deformation as follow.

$$J = J_e + J_p \tag{1}$$

where the elastic component, J_e, is given by

$$J_e = \frac{K_I^2}{E'} \tag{2}$$

here, K_I is the elastic stress intensity factor and E′ = E or $E' = E/(1-\nu^2)$ whether plane stress or plane strain conditions are assumed with E representing the (longitudinal) elastic modulus [14].

The plastic component, J_p, can be conveniently evaluated from the fully plastic solution of a strain hardening material introduced by Shih and Hutchinson [11] and further validated by Kumar et al. [10]. For an elastic–plastic material following a Ramberg-Osgood model [14,15] to describe the uniaxial true stress ($\bar{\sigma}$) vs. logarithmic strain ($\bar{\varepsilon}$) response given by

$$\frac{\bar{\varepsilon}}{\varepsilon_0} = \frac{\bar{\sigma}}{\sigma_0} + \alpha\left(\frac{\bar{\sigma}}{\sigma_0}\right)^n \tag{3}$$

where σ_0 is the normalizing stress, $\varepsilon_0 = \sigma_0/E$ is the normalizing strain, α is a dimensionless constant, n defines the strain hardening exponent, the fully plastic J_p is expressed as

$$J_p = \alpha b \sigma_0 \varepsilon_0 h_1\left(\frac{a}{W}, \mathscr{L}, n\right)\left(\frac{P}{P_0}\right)^{n+1} \tag{4}$$

where a is the crack size, W is the specimen width, $b = W - a$ defines the uncracked ligament, $\mathscr{L}$ represents the characteristic length, P is the generalized load, and P_0 is the corresponding limit load. In the above expression, h_1 is a dimensionless factor which depends on crack size, geometry, and strain hardening properties. The previous solution for J_p is essentially applicable for fully plastic cracked configurations in which the elastic strains are vanishingly small, particularly within the annular region surrounding the crack-tip where the condition $J \propto P^{n+1}$ holds true. To introduce an estimation procedure for J_p in a pipe having a circumferential surface crack located at the girth weld centerline subjected to bend loading (as depicted in Fig. 1), the mismatch (M_y) ratio must be defined in the form

$$M_y = \frac{\sigma_0^{WM}}{\sigma_0^{BM}} \tag{5}$$

where σ_0^{BM} and σ_0^{WM} denote the reference stresses of the parent and weld metals, respectively. It is convenient express the current methodology in terms of weld metal rather than base material, thus the effect of weldments can be taken into account explicitly. Eq. (4) is rewritten as follows

$$J_p = \alpha b \sigma_0^{WM} \varepsilon_0^{WM} h_1\left(\frac{a}{t}, \frac{D_e}{t}, \theta, M_y, n^{WM}\right)\left(\frac{M}{M_0^{WM}}\right)^{n^{WM}+1} \tag{6}$$

Here, D_e is the pipe (cylinder) outer diameter, t is the wall thickness, $b = t - a$ now defines the uncracked ligament, M denotes the applied bending moment, WM superscript denotes mechanical properties related to weld metal, and the surface crack length is described by the angle θ (see Fig. 1) [12,16]

$$\theta = \frac{\pi c}{2D_e} \tag{7}$$

where c is the circumferential crack half-length. In the above expression, the limit bending moment M_0^{WM}, is also defined in terms of the weld metal and conventionally is given by Refs. [12,16]

$$M_0^{WM} = 2\sigma_0^{WM} R_m^2 t\left(2\sin\beta - \frac{a}{t}\sin\theta\right) \tag{8}$$

in which R_m denotes the mean radius ($R_m = (R_e + R_i)/2$ where R_e and R_i are the external and internal radius) and the parameter β is defined as

$$\beta = \frac{\pi}{2}\left[1 - \left(\frac{\theta}{\pi}\right)\left(\frac{a}{t}\right)\right] \tag{9}$$

The limit solution for the bending moment given by Eq. (8) is applicable in the range ($\theta + \beta \le \pi$) [12,16]. Here, it is clear that the previous Eq. (8) corresponds to the limit load solution applicable for a circumferentially-oriented surface crack in girth weld pipe made of weld metal flow properties (reference stress, σ_0^{WM}, and its associated strain hardening exponent, n^{WM}). This condition is often referred to All Weld Metal (AWM) configuration. Use of Eq. (8) proves to be convenient in current FFS applications since the limit bending moment, M_0, in Eqs. (6) and (13) can be viewed just as a normalizing parameter which would only affect the value of factor h_1 (h_4) but not the net value of J_p (δ_p).

The previous framework also applies when the CTOD is adopted to characterize the crack-tip driving force. Following the earlier analysis for the J-integral and using the connection between J and CTOD (δ) [17,18] given by

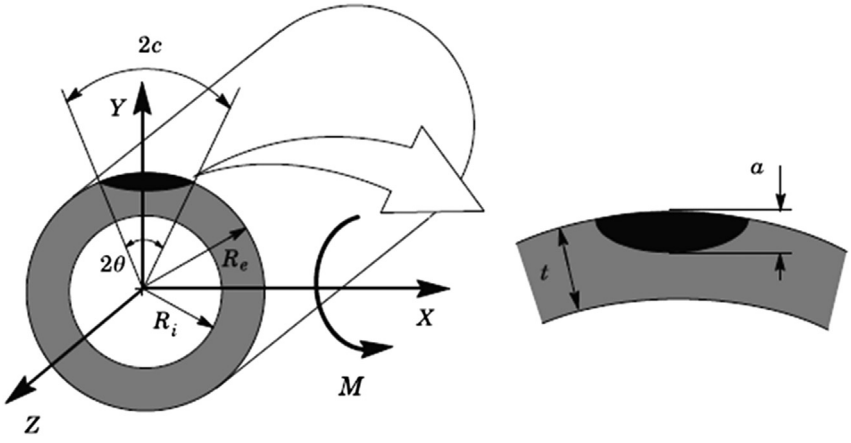

Fig. 1. Defective pipe configuration employed in the numerical analyses.

$$\delta = \frac{J}{m\sigma_0^{WM}} \tag{10}$$

in which m is a dimensionless constant. Consequently, a similar formal expression to Eq. (1) is employed to yield

$$\delta = \delta_e + \delta_p \tag{11}$$

where the elastic component, δ_e, is given by

$$\delta_e = \frac{K_I^2}{m\sigma_0^{WM}E'} \tag{12}$$

and the plastic component, δ_p, is expressed as

$$\delta_p = \alpha b \varepsilon_0^{WM} h_4\left(\frac{a}{t}, \frac{D_e}{t}, \theta, M_y, n^{WM}\right)\left(\frac{M}{M_0^{WM}}\right)^{n^{WM}+1} \tag{13}$$

where h_4 now defines a dimensionless factor dependent upon crack size, component geometry, strain hardening properties, and mismatch level. It follows from the previous relationship between J and CTOD given by Eq. (10), that $h_4{=}h_1/m$ when $J_p \gg J_e$(and, equivalently, $\delta_p \gg \delta_e$). On the other hand, CR [13] provides additional results to support the validity of this relationship for cracked configurations analyzed here. Finally, the elastic terms, J_e and δ_e are calculated by using Eqs. (2) and (12) coupled with a convenient form of the elastic stress intensity factor, K_I. For a circumferential surface crack in a pipe subjected to a (pure) bending moment, an improved expression for this parameter is given by Ref. [16]

$$K_I = \sigma_b G_5 \sqrt{\frac{\pi a}{Q_s}} \tag{14}$$

where σ_b is the (global or net-section) bending stress about the X-axis (see Fig. 1) expressed as

$$\sigma_b = \frac{4MR_e}{\pi\left(R_e^4 - R_i^4\right)} \tag{15}$$

with the flaw shape parameter, Q_s, is defined as

$$Q_s = 1 + 1.464\left(\frac{a}{c}\right)^{1.65} \quad ; a \le c \tag{16}$$

In the above expression Eq. (14), G_5 is the influence coefficient corresponding to a circumferential, semi-elliptical surface crack in a cylinder subjected to a (pure) net-section bending as given in Appendix C of API 579 [16]. Current available solutions [10,12,13] provide a complete set of tabulated h factors for structural components made completely of base metal and does not consider bimetallic components. The accuracy of the proposed solutions will depend on how h parameters are computed from numerical simulations for the mismatched pipe at the crack-tip level. The applicability analysis, described below, shows a window where the proposed scheme works well in terms of mismatch level and crack dimensions regardless weld groove size. Further, the proportionality concept between quantities, which is the basis of the EPRI approach, is also evaluated by means of two key configurations with various levels of overmatch having both moderate and low strain hardening materials as base plate. The following sections explore in detail the numerical analysis and validation procedure to estimate J and CTOD measures in welded defective pipes.

3. Numerical procedures and finite element models

3.1. 3D models of girth-welded pipes with circumferential cracks

Nonlinear finite element analyses are described for 3D models of cracked girth weld pipes subjected to bending load. The analyzed pipe models have a wall thickness $t = 20.6$ mm with weld groove width $2h = 15$ mm, and different external diameters $D_e = 206$ mm ($D_e/t = 10$), $D_e = 309$ mm ($D_e/t = 15$), and $D_e = 412$ mm ($D_e/t = 20$). These geometries typify current trends in high pressure, high strength pipelines, including submarine pipelines and risers. The analysis matrix considers weld centerline surface flaws with varying crack depth (a) and crack length ($2c$) as defined by $a/t = 0.1$ to 0.5 with increments of 0.1 and $\theta/\pi = 0.04$, 0.12 and 0.20 ($1.7 \le c/a \le 82.5$ – see Eq. (7)). Fig. 1 shows the pipe configuration and defect geometry adopted in the simulations. The effect of weld groove size on crack-tip driving forces is also evaluated by varying the weld width in the range 15 mm < $2h$ < 41.6 mm ($h/t = 0.36$, 0.50 and 1.0 where t is considered constant for all analyses).

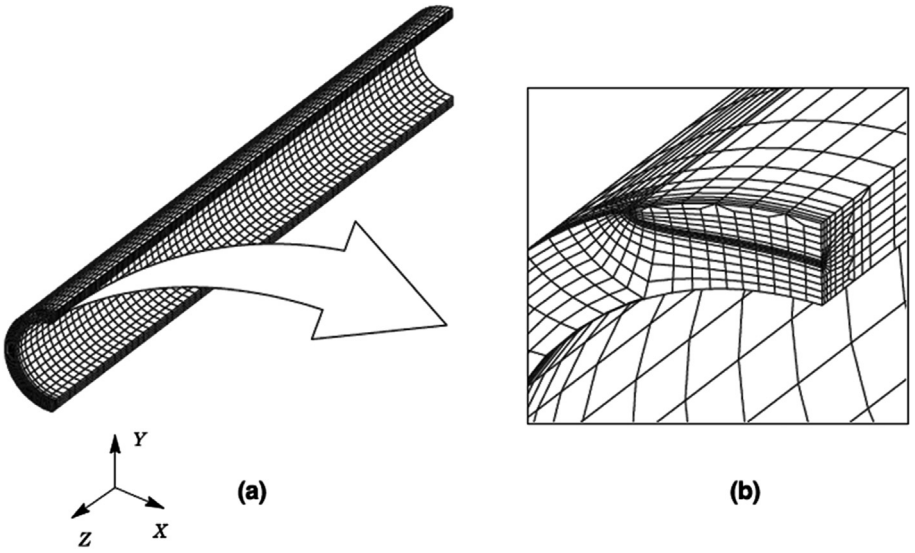

Fig. 2. 3D finite element model employed for the pipe configuration with $D_e/t = 10$, $a/t = 0.5$ and $\theta/\pi = 0.12$; (a) Global description; (b) Local near-tip model and meshing details.

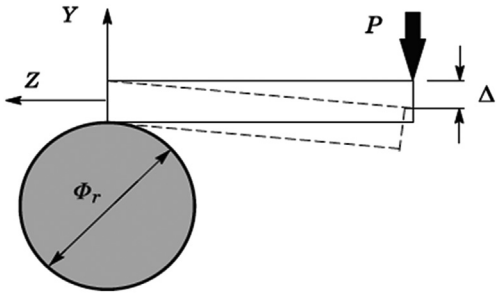

Fig. 3. Proposed reeling process scheme for numerical simulations.

Fig. 2a, b illustrates the finite element model constructed specifically for a pipe with $D_e/t = 10$, $a/t = 0.5$ and $\theta/\pi = 0.12$. A focused ring of elements surrounding the crack front is used to shape a small key-hole geometry (blunt tip) as crack tip whose radius is $\rho_0 = 5$ μm (0.005 mm). The crack front is described by 15 (semi-elliptical) layers defined over the crack half-length (c); the thickest mesh layer is located at the deepest point of the crack and the free surface of pipe is composed by an arrangement of thinner mesh layers in order to accommodate the strong stress gradient distributed along the crack front. Symmetry conditions permit modeling a quarter of the pipe with appropriate constraints imposed on the remaining crack ligament and symmetry plane. A typical quarter-symmetric girth weld pipe model with a crack has about 15,000 8-node 3D elements and 18,000 nodes. The boundary conditions imposed on the finite element model resemble the four-point bending scheme in which the bending moment is constant and the shear force is null at the crack plane. Very similar numerical models were employed for other cracked configurations. Likewise, 3D finite element models were constructed to simulate the loading condition of the pipe when is subjected to reeling method. Fig. 3 illustrates a simplified scheme of reeling method to describe the evolution of J integral when the pipe is coiled around the reel drum. The cylinder is modeled as a rigid surface and the pipe length is long enough to ensure fully contact with it. Further details such as geometric features and main dimensions are given in Section 6. The FE models were initially verified by means of linear elastic fracture mechanics approach (LEFM) through Eqs. (2) and (14). The computed J_e derived from the contours definition (given in the next sub-section) in numerical simulations is converted to K_I by means of Eq. (2) and then compared to its tabulated value given by Eq. (14) [16]. All the differences between numerical results and tabulated values fall in the range of less than 1%.

3.2. Solution procedures and material models

The finite element code WARP3D [19] provides the numerical solutions for 3D analysis reported here. The code enables conventional elastic–plastic analysis with Mises (J_2) plasticity constitutive model for both small-strain and finite-strain theory. Evaluation of the J-integral follows a domain integral procedure [20], which leads to very consistent values for several distant contours from the crack-tip. Thus, it retains a strong independent path for domains defined outside the highly strained material near the crack tip. The "through-thickness" average J is computed over domains defined well outside of the crack-tip, where, otherwise, the highly non-proportional histories of the near-tip fields would affect path independency of the line integral. Likewise, the numerical evaluation of CTOD needed to compute the h_4 factor follows similar technique employed previously for determining J values. The widely used 90° intercept procedure is performed to compute numerical values of CTOD. In order to avoid a highly distorted mesh in the crack flank region, a linear curve fitting is used through the nodes of the crack face to render the undeformed opening crack flank. Thus, an intersection point is created between this line and a 45° (due to symmetry) secant line which was originated from the crack-tip node. Then, CTOD is measured. This strategy suppresses the ambiguity to determine CTOD at the crack tip in severe mesh distortion (For more details see Refs. [13,22]). 3D FE simulations of the reeling method are performed using the standard penalty method [19] on the contact surface between the pipes and reeling drum modeled as a rigid cylinder (see Fig. 3).

Evaluating factors h_1 and h_4 require nonlinear finite element solutions that include effects of remote loading as well as weld strength mismatch on J and CTOD. Therefore, they utilize the elastic–plastic constitutive model with flow theory and conventional Mises plasticity in small geometry change (SGC) settings. The numerical solutions employ a simple power-hardening law to characterize the uniaxial stress ($\overline{\sigma}$) vs. strain ($\overline{\varepsilon}$) in the form

$$\frac{\overline{\varepsilon}}{\varepsilon_0} = \frac{\overline{\sigma}}{\sigma_0} \quad ,\overline{\varepsilon} \le \varepsilon_0 \quad ;\frac{\overline{\varepsilon}}{\varepsilon_0} = \alpha\left(\frac{\overline{\sigma}}{\sigma_0}\right)^n \quad ,\overline{\varepsilon} > \varepsilon_0 \tag{17}$$

where σ_0 is the normalizing stress, $\varepsilon_0 = \sigma_0/E$ is the normalizing strain, α is a dimensional parameter (for simplicity is kept constant for all analyses, $\alpha = 1$) n is the strain hardening exponent.

The mismatched configurations have material flow properties, which cover a relatively wide range of weld strength mismatch: evenmatch and 10%, 20%, 30% and 50% overmatch ($M_y = 1.0, 1.1, 1.2, 1.3$ and 1.5, respectively – see Eq. (5)). The weldments are modeled as a bimetallic system (the heat affected zone, HAZ, is not considered in the present work) with fixed yield strength and hardening exponent for each base plate set. The mechanical properties of the base metal were varied according to typical range of high strength low alloy (HSLA) steels as: $n = 5$ and $E/\sigma_0 = 800$ (high hardening material), $n = 10$ and $E/\sigma_0 = 500$ (moderate hardening material), $n = 20$ and $E/\sigma_0 = 300$ (low hardening material). Table 1 provides the material properties used in this work for fractured pipes with square groove welds, which also consider $E = 206$ GPa and $\nu = 0.3$. The corresponding hardening exponents for each weld metal are determined by a linear interpolation between the normalizing stress and flow properties (E/σ_0 and n) given by previous tabulated values. This set of properties reflects the upward trend of the yield strength and the hardening exponent, which are characteristics of ferritic steels.

In the present study, the calculation of h_1 factor follows an evaluation procedure, where it is derived from the slope of a least square fit to the linear evolution between $J_p/(\alpha\sigma_0^{WM}\varepsilon_0^{WM}b)$ and $(M/M_0)^{n^{WM+1}}$ (It is similar for evaluating h_4). Section 4 addresses this issue in more detail for the analysis of girth weld pipes. The procedure requires the specification of the ultimate tensile strength, σ_{uts}, to determine the level of J (and CTOD) at which the limit bending moment, corresponding to instability of the crack ligament, is attained. For instance, it is assumed that the rising

Table 1
Material properties adopted for the analyses of weldments.

Mismatch level	High hardening		Moderate hardening		Low hardening	
	σ_{ys}^{WM} (MPa)	n^{WM}	σ_{ys}^{WM} (MPa)	n^{WM}	σ_{ys}^{WM} (MPa)	n^{WM}
Evenmatch/Base Plate	258	5.0	412	10.0	687	20.0
10% Overmatch	284	5.8	453	11.5	755	22.5
20% Overmatch	309	6.7	494	12.8	824	25.0
30% Overmatch	335	7.5	536	14.5	893	27.5
50% Overmatch	386	9.5	618	17.4	1030	32.5

plastic zone size at the crack-tip (due to increased applied load) is well contained by the weld strip in all the way of plastic deformation. Hence, stable or unstable crack growth is expected to occur at some point before the yielding zone reaches the base material (fusion line). Thereby, the flow properties of filler material would control the fracture process like whether the pipe would be made of all weld metal (AWM). Each welding material property set, σ_{uts}^{WM} is estimated using the following relationship [16]

$$\sigma_{uts}^{WM} = \sigma_0^{WM}\left[\frac{\left(\frac{500}{n^{WM}}\right)}{e^{(1/n^{WM})}}\right] \tag{18}$$

In order to validate the proposed set of solutions, a detailed finite element simulation is performed using an API 5L X60 [21] pipeline steel with 483 MPa yield stress at room temperature (20 °C) and relatively high hardening properties ($\sigma_{uts}/\sigma_0 \approx 1.24$), where σ_{uts} is the ultimate tensile strength as depicted in Fig. 4 tested by Ref. [23]. The girth weld size ($2h$) as well as the overmatching level was selected arbitrarily considering the above material properties as fixed base plate. A simpler linear interpolation was carried out in order to obtain adequate mechanical parameters (σ_0^{WM}, n^{WM}) for each level of weld strength mismatch as described in Table 1.

4. Applicability and limitations of *J* and CTOD estimation procedures

J and CTOD estimation procedures for defective girth weld pipes, based on fully plastic solutions pose certain difficulties at the instant to assess structural integrity. Since the level of mismatch might affect the near-tip stress and strain fields in welded components, the fracture parameters like *J* (CTOD) might not be scaled directly with the applied loading. One of the basic requisites is the proof consistency between field quantities and external applied force, where both measures are intrinsically linked by a linear proportional relationship. In other words, the stresses and strains within the singularity region increase in direct proportion to the bending moment in a heterogeneous media. CR [13] has provided an extensive analysis regarding this aspect as well as other key issues which have direct bearing with robustness of the present methodology applicable to similar cracked pipes in homogeneous condition. In the following subsections, the conditions to ensure confidence of the present results will be addressed through a detailed finite element analysis. Firstly, will be considered mismatched components with high strain hardening materials ($n \leq 10$) as parent material. The weld strength and hardening exponent are calculated from Table 1. Then, three coupled effects between weld strength mismatch and material-geometrical pipe properties are investigated for key configurations having different weld groove sizes and pipe diameters. Secondly, a similar procedure, but more shortly, is performed to low strain hardening ($n \geq 20$) configurations. The outcome of applicability analysis determines the range on which the crack-tip driving forces simply scale with the applied load in welded structures that gives a better understanding of the coupled effects associated with mechanical properties of filler metal.

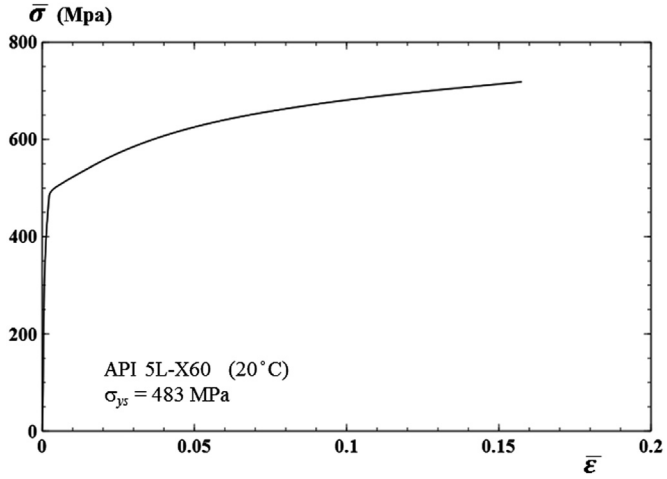

Fig. 4. Uniaxial true stress-true strain curve for API X60 steel having continuous hardening.

4.1. Coupled effect of weld strength mismatch and hardening behavior

The simple functional dependence of the field quantities on the applied bending moment or displacement also means that quantities such as the *J*-integral, CTOD and other crack parameters have the form given by Eqs. (6) and (13), respectively. The Eq. (6) can be rearranged by applying logarithms in both sides of equation and neglecting the factor dependence h_1 and other constants (analogous procedure is for computing h_4 from CTOD), the resulting functional form follows

$$\log J_p = \left(n^{WM}+1\right)\log\left(\frac{M}{M_0^{WM}}\right) \tag{19}$$

where the hardening exponent plus unity becomes the slope of the evolution of crack driving force with respect to the normalized applied bending moment. Once the fully plastic condition is attained ($M/M_0^{WM} \geq 1$) along the uncracked ligament, the J_p evolution follows a linear proportional variation irrespective to the plastic deformation. In some cases the slope of the linear increment does not match with the proposed criterion defined by Eq. (19), might be because the near-tip plastic zone is well contained within the weld strip (shielding effect) or bimetallic configurations with low hardening materials. The shielding effect is produced by high levels of overmatch in the weld material that leads to the occurrence of plastic zones at remote places far from the fracture zone (Heat affected zone or fusion line) and thus protecting the welded joint.

Fig. 5 illustrates the variation of $\log J_p$ with respect to $\log(M/M_0^{WM})$ for both moderate and lower strain hardening materials (n^{BM}=10, 20) as parent materials, including different cracked pipe geometries and various weld strength mismatch levels. Here, the weld half-width to thickness ratio ($h/t = 0.36$; $2h = 15$ mm) is considered constant as well as the circumferential crack length ($\theta/\pi = 0.2$). The adopted crack depth and outer pipe diameter represent the combination of shallow and deep cracks ($a/t = 0.2, 0.5$) with pipes of medium and large sizes ($D_e/t = 10, 20$). Besides, a number of reference lines were added on the graphs with slopes (n^{WM}+1) corresponding to each overmatched level. In Fig. 5a the actual slope of J_p with $\log(M/M_0^{WM})$ almost matched with the slope of the reference line at the beginning of the yielding condition ($\log(M/M_0^{WM}) = 0$) in evenmatch weldment. However, the more the overmatch level increases, the more the J_p deviation will be with respect to its reference line. For 50% overmatch configuration, the proportional increment between quantities unmistakably is no longer valid due to excessive deviation observed in all the way of plastic deformation. Considering this approach as an engineering solution, the 30% overmatch condition still has a large portion of J_p mounted on the reference line given by Eq. (19). Similar behavior is observed in Fig 5b, but somewhat different from the previous one

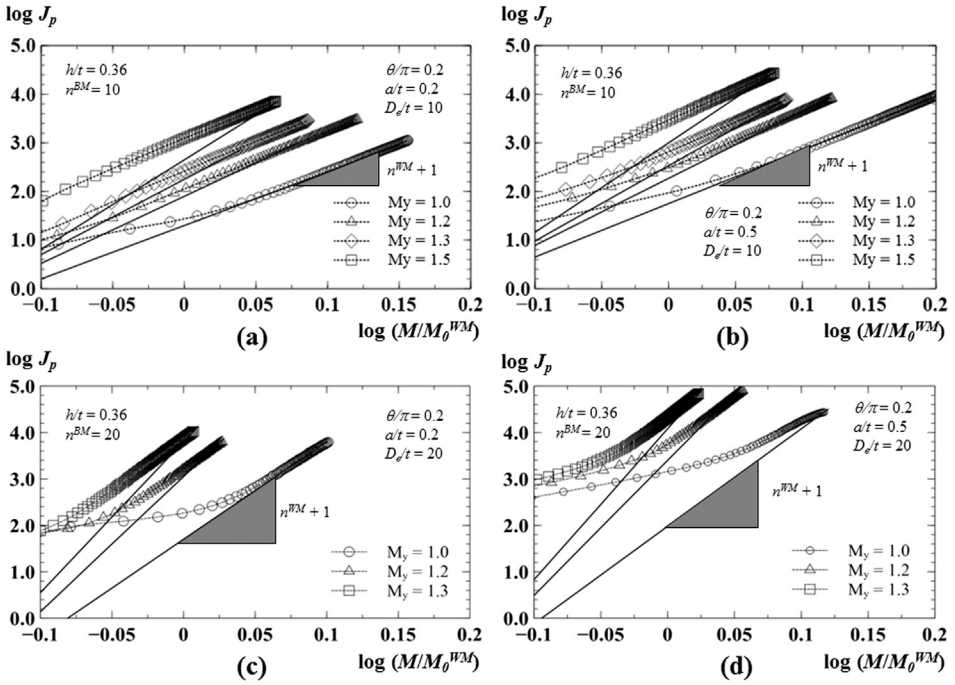

Fig. 5. Proportionality test of J integral and applied bending moment for circumferentially surface cracks in girth weld pipes including various weld strength mismatch and crack lengths; (a) $n^{BM} = 10$, $D_e/t = 10$, $\theta/\pi = 0.2$, $a/t = 0.2$; (b) $n^{BM} = 10$, $D_e/t = 10$, $\theta/\pi = 0.2$, $a/t = 0.5$; (c) $n^{BM} = 20$, $D_e/t = 20$, $\theta/\pi = 0.2$, $a/t = 0.2$; (d) $n^{BM} = 20$, $D_e/t = 20$, $\theta/\pi = 0.2$, $a/t = 0.5$.

for deep crack pipe. These results clearly express the univocal relation between crack-tip fields and the applied bending moment regardless the crack geometry nor pipe dimensions for relatively low levels of overmatch ($M_y \leq 1.3$). Likewise, in welded pipes having high strain hardening materials ($n^{WM}=5$) as parent metal, the crack driving forces are also associated to the stress and strain fields given by the HRR singularity at the crack-tip region [9–13]. The outcomes derived from that analysis are not presented here for the sake of the available space, but are also applicable for the same level of mismatch in cracked pipes described above.

For low hardening base plate materials, Eq. (19) is strongly compromised due to a large amount of elastic strain energy present mainly in the initial stage of loading and barely in the plastic regime causing a strong divergence with respect to the reference line. However, after certain plastic deformation, the J_p evolution follows the reference slope being more prominent for shallow crack ($a/t = 0.2$) rather than deep crack ($a/t = 0.5$) configurations for $M_y = 1.0 - 1.3$ as shown in Fig. 5c and d, respectively. Nevertheless, the EPRI J seems to be invalid when the level of overmatch exceeds 30% ($M_y > 1.3$) and the assumed linear variation is not conserved. In particular, this is observed in materials which exhibit a lower ability to deform plastically, and thus the elastic contribution to the strain energy could drive to a failure mechanism distinct from ductile fracture. Therefore, 50% overmatch configurations will be considered as test values in the following analyses in order to provide a limiting value regarding applicability of this methodology. But, it will not be included as part of solutions presented in Section 5. Likewise, the dependence of the h_4 factor on CTOD has similar values whereby are not shown here. Overall, these results suggest that this method is suitable for bimaterial configurations with moderate to high hardening baseplate materials. Conversely, this would be a poorly predictive method in welded components having parent metals with low hardening properties.

The correct determination of h factors depends on how the parameters are computed from the FE analysis unambiguously. The aforementioned procedure adopts the principle of proportionality between field quantities and applied loading to prove J dominance at the crack-tip; hence, same assumption is also applied to compute the dimensionless h_1 through Eq. (6) rewritten in the following form

$$\bar{J}_p = \frac{J_p}{\alpha \varepsilon_0^{WM} \sigma_0^{WM} b} = h_1\left(\frac{a}{t}, \frac{D_e}{t}, \theta, M_y, n^{WM}\right)\left(\frac{M}{M_0^{WM}}\right)^{n^{WM}+1} \quad (20)$$

where h_1 factor is a function of crack geometry, pipe dimensions and mechanical properties of the welded pipe. Fig. 6 exhibits the actual scheme used to compute such coefficients of both moderate and low hardening parent materials. In evenmatch condition the quantities vary each other linearly, whereby its slope is constant all the way of deformation. Thus, h parameter can be calculated through the functional dependence given by Eq. (20). On the other hand, the linear trend turns into nonlinear as result of increasing of mismatch levels on the weldment making quite complicated the determination of a unique slope. A least square regression line is used to define a linear region where the slope is derived as well as h factor. The region is delimited by the normalized bending moments $(M/M_0^{WM})^{n^{WM}+1}$ at the initiation of yield condition (σ_0^{WM}) as lower limit and the ultimate tensile strength (σ_{uts}^{WM}) as upper limit. The corresponding limit bending moment for weld metal is given by Eq. (8) and the ultimate tensile strength is defined by Eq. (18). Therefore, the computed h factor is extracted from a strain range which is more realistic in terms of load-carrying capacity and deformation levels, thereby given confidence in the present results.

4.2. Coupled effect of weld strength mismatch and pipe diameter size

The robustness of a single parameter to characterize fracture process in the vicinity of the crack-tip relies upon the strong connection between geometric local parameter (CTOD) and J integral [18]. Despite of heterogeneity's nature of weldments, Joch and Ainsworth [24] proved that J and CTOD's connection is still

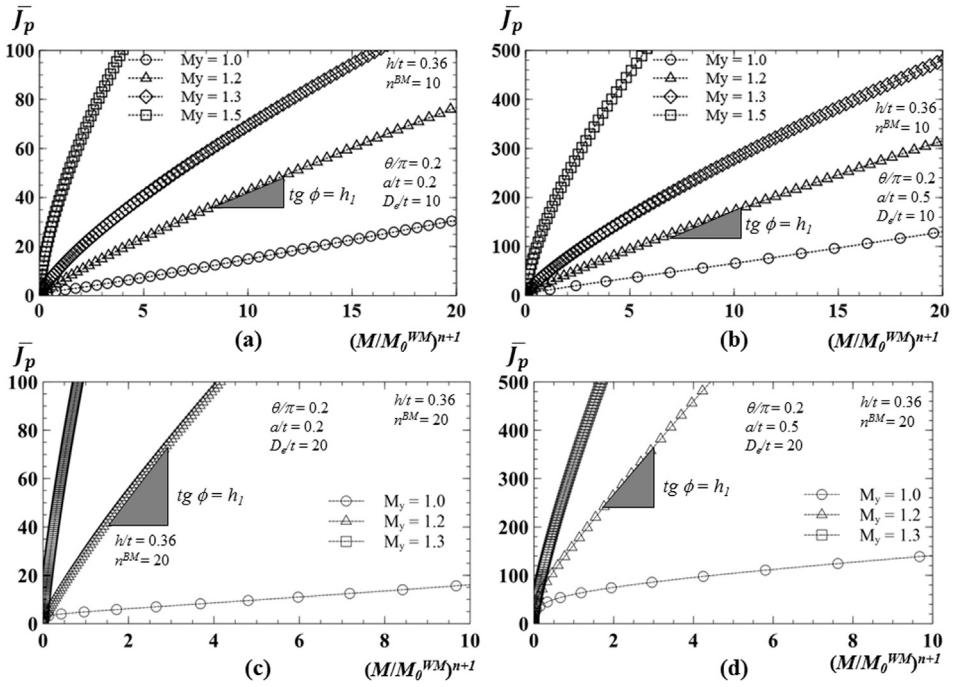

Fig. 6. Numerical approach adopted to determine h factors from evolution of J with respect to normalized applied bending moment; (a) $n^{BM} = 10$, $D_e/t = 10$, $\theta/\pi = 0.2$, $a/t = 0.2$; (b) $n^{BM} = 10$, $D_e/t = 10$, $\theta/\pi = 0.2$, $a/t = 0.5$; (c) $n^{BM} = 20$, $D_e/t = 20$, $\theta/\pi = 0.2$, $a/t = 0.2$ (d) $n^{BM} = 20$, $D_e/t = 20$, $\theta/\pi = 0.2$, $a/t = 0.5$.

conserved in some bimaterial configurations with certain restrictions. For instance, a weldment behaves as a single weld material when the strip dimension ($2h$) surpasses the remaining ligament (b) in length and otherwise when it is too small and the fracture process is controlled by flow properties of the base material. In this subsection were carried out a number of finite element analyses with various crack dimensions and material properties to evaluate the coupled effect of weld strength mismatch and pipe diameter size on d_n. The dimensionless parameter d_n ($\equiv 1/m$) is derived from Eq. (10) and conveniently can be expressed in terms of h factors through Eqs. (6) and (13) in the form of $h_4 = d_n h_1$.

Figs. 7 and 8 depict the variation of d_n with respect to different cases (θ/π, a/t and h/t -ratios -see Table 2) for moderate and low strain hardening base material. These are grouped in various weld strength mismatch levels and pipe diameter to thickness ratio. For instance, the resulting d_n certainly display an independence trend from configurational effects and material properties for all cases in evenmatch conditions as shown in Figs. 7 and 8a, where it is possible to relate them with a straight line. Here, for moderate hardening material the $d_n \approx 0.6$ and for low hardening material $d_n \approx 0.7$, respectively. These results are quite compatible with those given in Ref. [18] for plane strain deformation in homogeneous materials. For $M_y > 1.0$, despite a few cases such as 4 to 6 (which present a slight deviation albeit insignificant from the linear tendency) in Fig. 7b and c, d_n still remains unrelated to configurational effects up to overmatch levels considered moderate ($M_y \approx 1.3$). Particularly, for these cases the coupled effect seems to be amplified by a combination of large circumferential crack extension (θ/π=0.12~0.2) and deeply cracked ($a/t \approx 0.5$) configurations, which vary in accordance to the strain hardening exponent of weld metal (n^{WM}). A distinct behavior occurs when higher levels of weld strength mismatch (M_y=1.5) are employed. The pipe diameter size and the mismatch ratio between weld and parent reference stresses can affect drastically the parameter d_n in all considered cases that lead to a loss of the equivalence between J and CTOD as illustrated in Fig. 7d. In similar form d_n varies strongly in defective weld pipes with low hardening material as base metal indicating a remarkable effect of weldments upon crack driving forces due to pipe dimension changes. Fig. 8b and c clearly show two almost constant values of d_n along the given cases for each D/t ratio, which means that it is almost insensitive to the crack dimensions and weld width (see Table 2) but depends on pipe size. Fig. 8d, however, displays a critical value $M_y = 1.3$ where the relationship between J and CTOD breaks down invalidating the concept of single parameter description. It is an open question as to whether J or CTOD is a characterizing parameter or indeed if either single parameter description is adequate. In this investigation the methodology is considered valid only if this equivalence prevails.

4.3. Coupled effect of weld strength mismatch and weld groove size

Fig. 9 displays the variation of h_1 factor with respect to increased mismatch levels (M_y) for circumferential surface flaws in girth weld pipes including $D_e/t = 10, 20$; $\theta/\pi = 0.04, 0.2$; $a/t = 0.2, 0.5$; and $h/t = 0.36$, 0.50 and 1.0 (where $t = 20.6$ mm, $2h = 15$, 20.6 and 41.2 mm, respectively). The base metal properties used to describe the present results corresponds to moderated hardening behavior. These results suggest that h/t has a negligible effect on near-tip fields when $M_y < 1.3$, whereby the functional dependence given by Eq. (6) is valid simply relating the crack geometry and material properties of weldment regardless the size of weld strip. Meanwhile, the increased weld strength mismatch produces nonlinear behavior of crack-tip forces that becomes relevant when the weld width is largest, specifically, for $M_y = 1.5$. The highest deviation of h_1 between $h/t = 0.36$ and 1.0 for $M_y = 1.3$ reaches 13–15% in all the given configurations. Same tendency is observed for other configurations with different parent materials ranging from lower to higher strain hardening properties (not presented here for the sake of the space). Therefore, overall, these results support the adopted procedure to estimate fracture mechanics parameters (J, CTOD) in circumferentially cracked-girth weld pipes in the range of

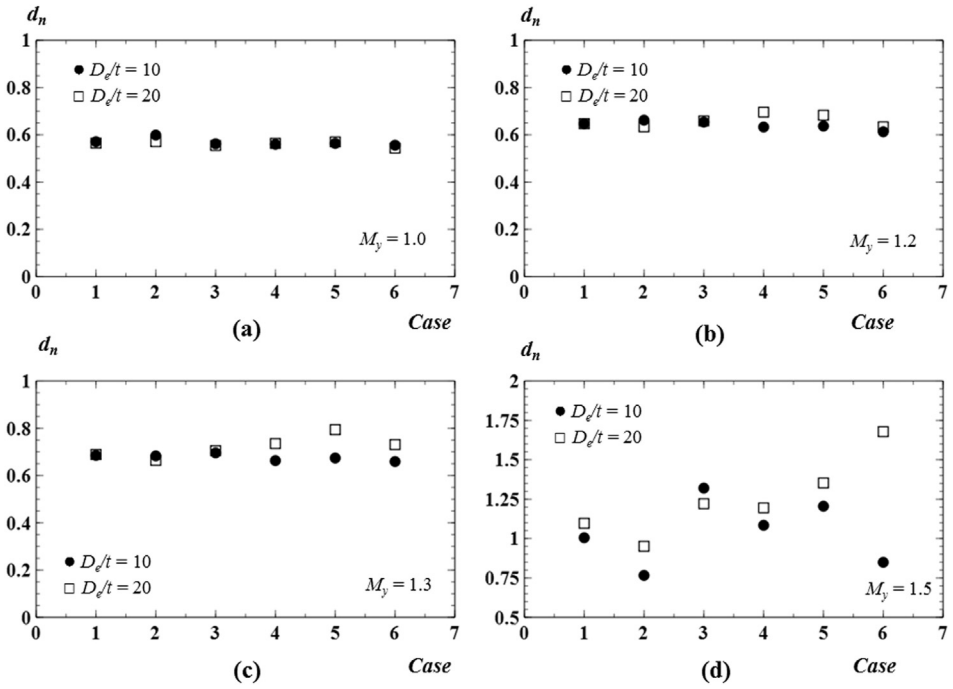

Fig. 7. Selected cases of coupled effect analyses between pipe diameter size and weld strength mismatch for $n^{BM} = 10$; (a) $M_y = 1.0$; (b) $M_y = 1.2$; (c) $M_y = 1.3$; (d) $M_y = 1.5$.

$1.0 \leq M_y \leq 1.3$ regardless of weld groove width when it is in the interval $0.36 \leq h/t \leq 1.0$.

5. *h* factors for circumferentially flawed girth weld pipes

Following previous outcomes related to applicability of J and CTOD estimation procedures based on a fully plastic framework, a definite set of solutions is constructed in which h_1 and h_4 dimensionless factor can be inferred directly from geometry parameters and mechanical properties of cracked girth weld pipes. Figs. 10, 11 provide solutions of h_1 and h_4 factors for high strain hardening base material (n^{BM}=5), Figs. 12, 13 for moderate hardening material (n^{BM}=10), and Figs. 14, 15 for low hardening material (n^{BM}=20), respectively. 3D coded color surfaces represents the set of solutions of each bimetallic configuration grouped by three different ratios of outer diameter to thickness (D/t). Each graph is

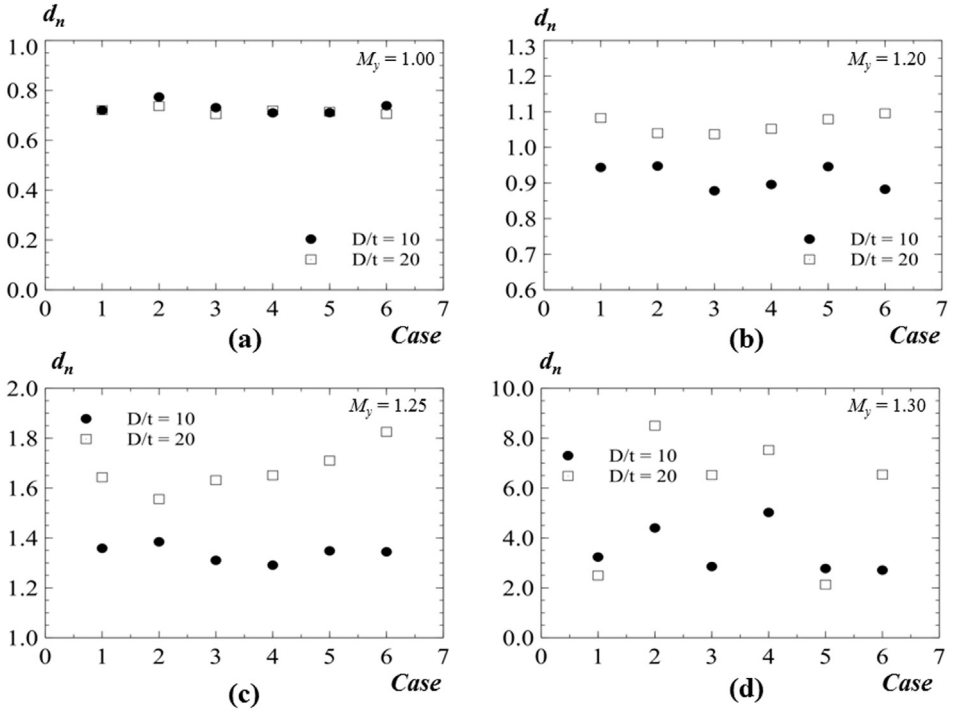

Fig. 8. Selected cases of coupled effect analyses between pipe diameter size and weld strength mismatch for $n^{BM} = 20$; (a) $M_y = 1.0$; (b) $M_y = 1.2$; (c) $M_y = 1.25$; (d) $M_y = 1.3$.

Table 2
Selected cases for evaluating the coupling between weld strength mismatch and pipe geometry.

Case	θ/π	a/t	h/t
1	0.04	0.2	0.36
2	0.04	0.5	1.00
3	0.12	0.2	0.36
4	0.12	0.5	1.00
5	0.20	0.2	0.36
6	0.20	0.5	1.00

composed by four 3D surfaces that correspond to each mismatch level, ordered in ascendant way for M_y = 1.0, 1.1, 1.2 and 1.3. The most suitable fitting equation for these surfaces was found by trial and error technique until the best correlation coefficients were obtained for each case. Therefore, a functional dependence is proposed in the form

$$h_{1,4} = \varsigma_0 + \varsigma_1\left(\frac{a}{t}\right) + \varsigma_2\left(\frac{a}{t}\right)^2 + \varsigma_3\left(\frac{a}{t}\right)^3 + \varsigma_4(\theta/\pi) + \varsigma_5\left(\frac{a}{t}\right)(\theta/\pi) + \varsigma_6(\theta/\pi)^2 \tag{21}$$

where ς_n are tabulated on Tables 3–8. Eq. (21) relates the h factor with D/t, a/t, θ/π and M_y within the following ranges: D/t = 10, 15, 20; $a/t = 0.1 - 0.5$ with increments of 0.1; $\theta/\pi = 0.04, 0.12, 0.20$; and $M_y = 1.0 - 1.3$.

There are some aspects about these results that should be pointed out. The surfaces, in particularly, are rising regarding the crack depth ratio, but are asymmetric with respect to θ/π=0.12. Beside, θ/π=0.12 also represents the point of maximum curvature. The outward normal vector describes a convex curvature that is quite marked for shallow cracks (a/t=0.1~0.2) at the extreme points of θ/π ratios (red-yellow color) and it is slightly marked for deep cracks (a/t~0.5) and large crack extensions (θ/π=0.12~0.2) – magenta color. For configurations that have parent material with high work hardening properties, the effect of weld strength mismatch is negligible compare to its evenmatch alternative for all considered D/t ratios as shown in Figs. 10, 11. All of them are almost mounted each other as if they were a single one. A plausible explanation about this behavior is the high dislocation density developed in the material when it is strained in excess of its yield point. The plastic straining generates new dislocations. As the dislocation density increases, further dislocation movement becomes more difficult since they hinder each other, which means the material hardness increases [14]. This reduces the plastic flow in the weld metal by the surrounding parent material which in turn would control the evolution of near-tip fields. Same steadily trending is conserved by relatively shallow cracks (a/t=0.1~0.3) when bimetallic components with moderate hardening behavior are employed. But, it changes drastically for deep crack configurations where the growing plastic zone is completely engulfed by the weld metal since the high constraint level built up by the surrounding material (Figs. 12, 13). However, the code color also suggests that crack length has a nil contribution on J and CTOD fracture parameters, particularly, for D/t = 10 and 15 where the color fringe remains almost constant along θ/π. Finally, Figs. 14, 15 illustrate 3D surfaces of h factors for low strain hardening materials. The maximum peak shifts from θ/π=0.12 to 0.04 for a/t = 0.5, where narrow but deep flaws seem to be prone to weld strength mismatch effect compared with other configurations. From this, following the color fringes, h factors reduce gradually in radial fashion until cracks become shallower (a/t=0.1~0.2). It turns out that the crack driving forces in weldments are comparable to those results from evenmatch conditions. But also note the highly order of magnitude reached by h factors for every overmatch levels (h_1=150~400; h_4=200~600). Fracture toughness, implicitly, is related to the yield strength of the material, crack dimension, geometry of the specimen and loading mode, including temperature threshold.

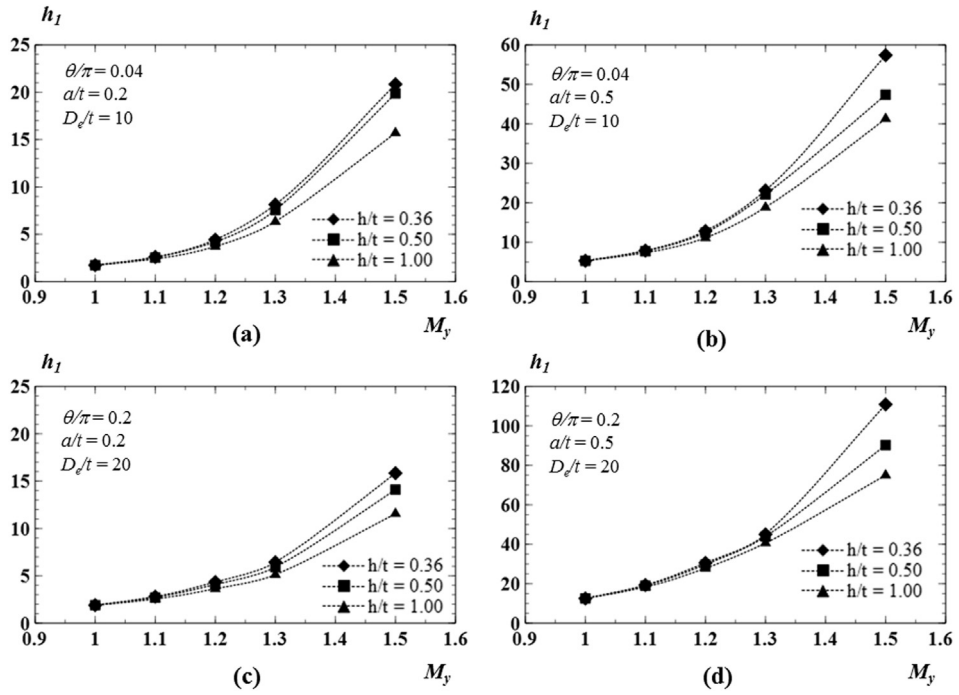

Fig. 9. Coupled effect of weld strength mismatch and weld groove size (h/t) ratio for n^{BM} = 10; (a) D_e/t = 10, θ/π = 0.04, a/t = 0.2; (b) D_e/t = 10, θ/π = 0.04, a/t = 0.5; (c) D_e/t = 20, θ/π = 0.20, a/t = 0.2; (d) D_e/t = 20, θ/π = 0.20, a/t = 0.5.

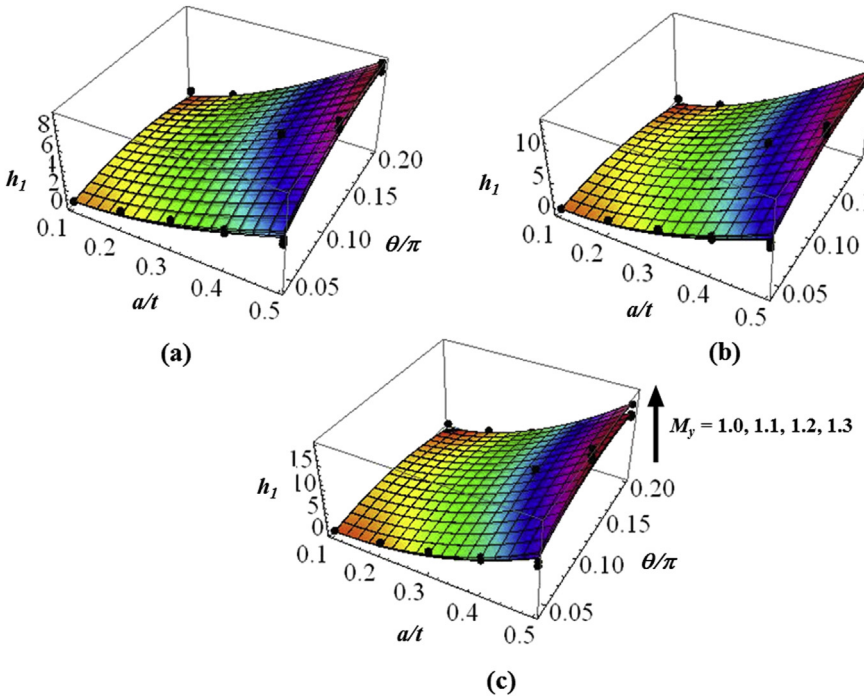

Fig. 10. 3D M_y surfaces of h_1 factor with increased a/t and θ/π for $n^{BM} = 5$; (a) $D_e/t = 10$; (b) $D_e/t = 15$; (c) $D_e/t = 20$.

However, in this investigation the configurational aspect of the pipe and loading mode remains constant but mechanically varied in accordance to a required mismatch level. It is clear, from these results, that the more the yield strength of the base plate is, the more the h values will be.

In heterogeneity conditions, the previous observations were basically kept regarding the trend and behavior of h factors applicable for welded configurations. Here, despite conserving the upward evolution for h factors with increased crack depth ratio (a/t), the growth rate is faster for deep cracks ($a/t > 0.4$) rather than shallow cracked pipe specimens as shown in Fig. 9b–d. A plausible explanation of such an effect is the high-grade of constraint attained by deep crack specimens around the crack-tip during the deformation process, which shows that the flow properties of the welding material drives the development of stress and strain fields. Therefore, h factors reveal a strong sensitivity to the coupled effect

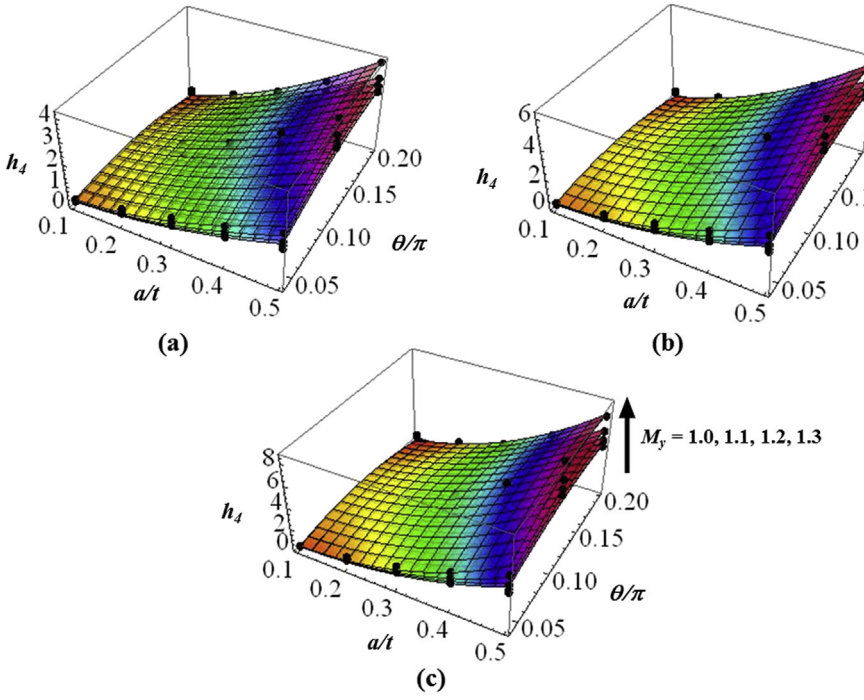

Fig. 11. 3D M_y surfaces of h_4 factor with increased a/t and θ/π for $n^{BM} = 5$; (a) $D_e/t = 10$; (b) $D_e/t = 15$; (c) $D_e/t = 20$.

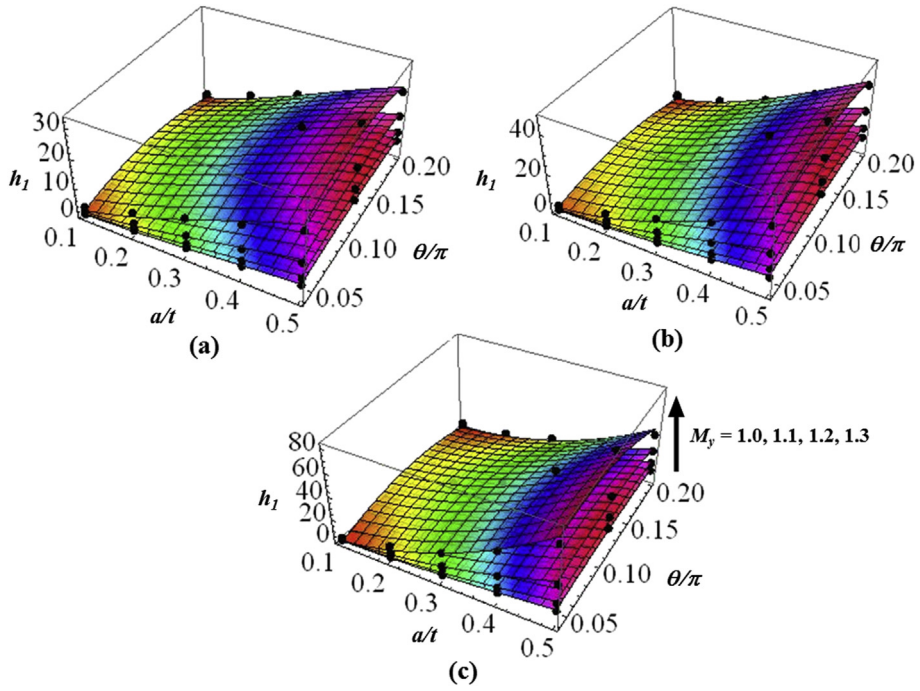

Fig. 12. 3D M_y surfaces of h_1 factor with increased a/t and θ/π for $n^{BM} = 10$; (a) $D_e/t = 10$; (b) $D_e/t = 15$; (c) $D_e/t = 20$.

of weld strength mismatch with crack geometry. This fact is also observed in similar fracture welded pipes as shown in Figs. 10–14.

6. Numerical simulations for cracked girth weld pipe under reeling deformation

Detailed 3D finite element analysis is conducted on circumferentially oriented surface flaws in girth weld pipe subjected to bending load, as shown in Fig. 3. The analyzed pipes geometry corresponds to typical steel catenary risers which are mostly used by offshore industry to extract oil and gas from seabed in deep-water. This study, particularly, considers a set of defective girth weld pipes with following characteristics: $D_e/t = 16.7$ ($D_e/t = 344.5$ mm, $t = 20.6$ mm), semielliptical surface crack face shape with length $2c = 100$ mm (θ/π=0.073), and different crack depths ($a/t = 0.1$ to 0.5 with increments of 0.1). A line pipe material API 5L

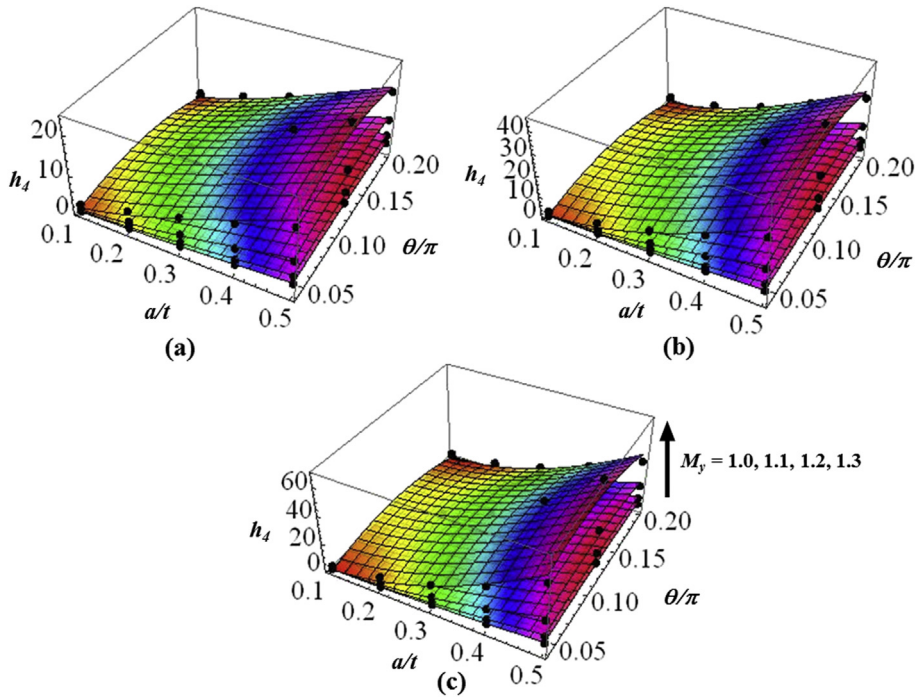

Fig. 13. 3D M_y surfaces of h_4 factor with increased a/t and θ/π for $n^{BM} = 10$; (a) $D_e/t = 10$; (b) $D_e/t = 15$; (c) $D_e/t = 20$.

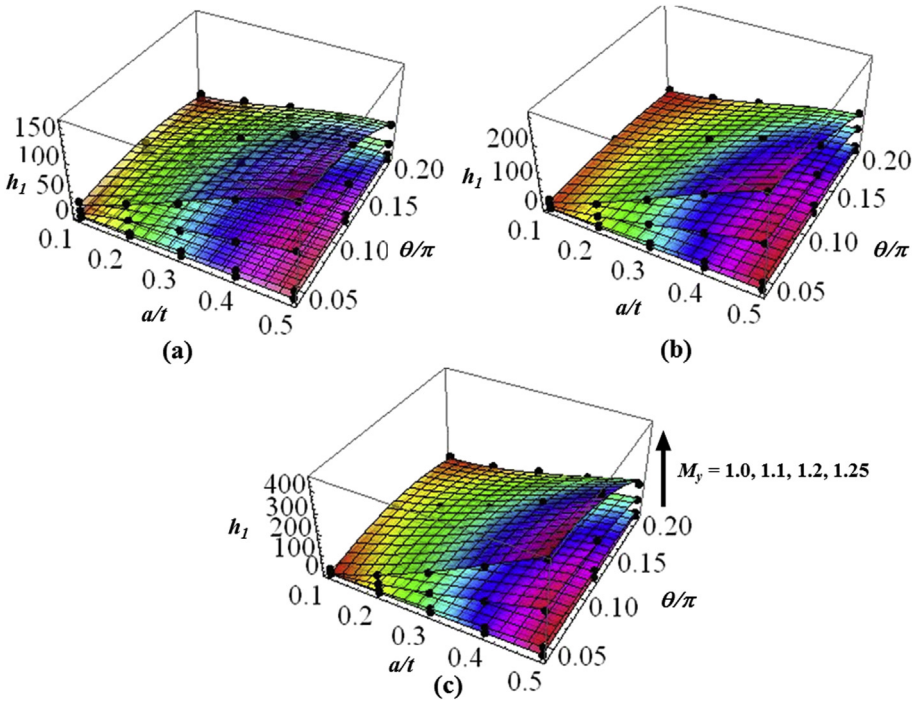

Fig. 14. 3D M_y surfaces of h_1 factor with increased a/t and θ/π for $n^{BM} = 20$; (a) $D_e/t = 10$; (b) $D_e/t = 15$; (c) $D_e/t = 20$.

X60 [23] is considered as a baseplate with its corresponding overmatched alternatives ranging from $1.0 < M_y < 1.25$. The corresponding yield stress and hardening exponent of each welded configuration is determined by means of a simple linear interpolation as explained in sub Section 3.2. The weld groove size is kept constant at a value of $2h = 25$ mm (h/t=0.61), which is less than the corresponding limiting value of $h/t = 1$, thus Eq. (21) is still applicable for such configurations.

The current FE analysis aims to predict the maximum J value attained by several crack dimensions in girth weld pipes while being spooled onto a large reel. Such condition is reached once a large portion of the longitudinal external surface of pipe makes

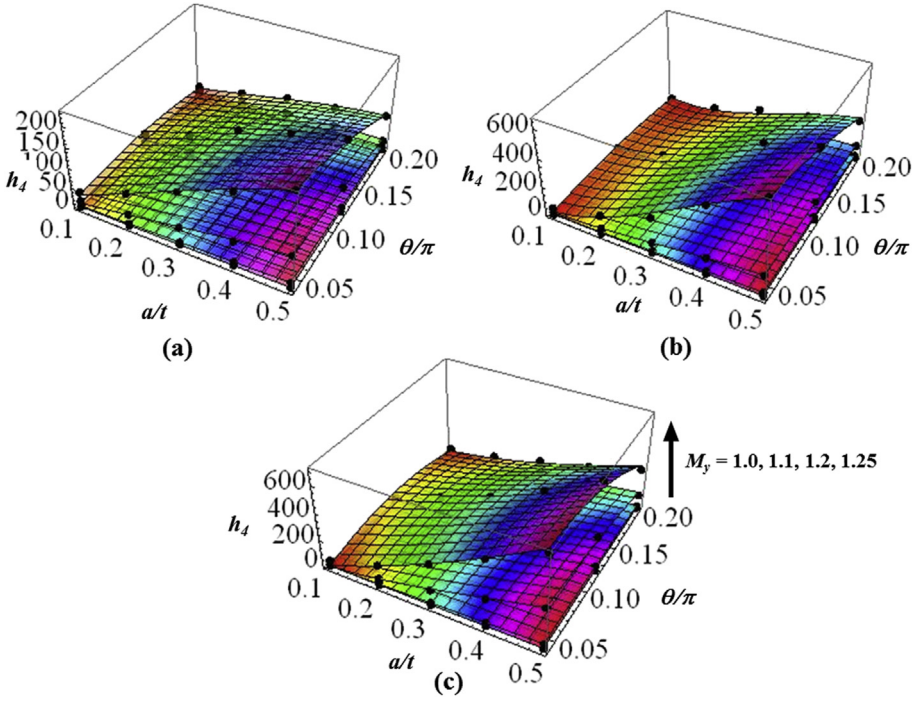

Fig. 15. 3D M_y surfaces of h_4 factor with increased a/t and θ/π for $n^{BM} = 20$; (a) $D_e/t = 10$; (b) $D_e/t = 15$; (c) $D_e/t = 20$.

Table 3
Coefficients of polynomial fitting of h_1 factor for mismatched configurations with high hardening base material.(n^{BM}=5, E/σ_0=800)

D_e/t	M_y	ζ_0	ζ_1	ζ_2	ζ_3	ζ_4	ζ_5	ζ_6	R^2
10	1.0	0.1429	−8.0064	39.5957	−18.0000	25.3078	62.6356	−148.3520	0.98
	1.1	0.2270	−8.3321	38.9077	−18.9694	22.7054	61.4994	−136.4360	0.98
	1.2	0.3265	−9.5696	42.5094	−23.3250	21.9719	62.6344	−133.8450	0.98
	1.3	0.3956	−10.4648	44.7876	−23.1056	23.5091	71.3880	−146.2120	0.98
15	1.0	0.1160	−15.3225	67.9638	−24.2611	39.0597	70.4044	−213.8730	0.97
	1.1	0.2862	−16.2215	68.2295	−27.7111	35.4674	73.2769	−200.1660	0.97
	1.2	0.4744	−18.3004	73.4738	−33.7333	34.4533	78.8456	−199.6470	0.97
	1.3	0.6350	−21.2407	82.5258	−38.2028	37.2902	91.1944	−219.6860	0.97
20	1.0	−0.8726	−12.7259	63.1632	6.5194	58.9531	55.2338	−291.1660	0.97
	1.1	−0.6547	−14.0988	63.0906	4.1583	55.4779	62.9244	−281.2140	0.97
	1.2	−0.3598	−16.6453	66.2075	2.9361	54.1983	75.2531	−285.0280	0.97
	1.3	−0.4830	−17.7105	66.2987	13.5806	61.1037	90.5575	−324.8330	0.97

Note: Polynomial fitting valid in the range $0.04 \le \theta/\pi \le 0.20$ and $0.1 \le a/t \le 0.5$.

Table 4
Coefficients of polynomial fitting of h_4 factor for mismatched configurations with high hardening base material.(n^{BM}=5, E/σ_0=800)

D_e/t	M_y	ζ_0	ζ_1	ζ_2	ζ_3	ζ_4	ζ_5	ζ_6	R^2
10	1.0	0.0164	−1.4584	8.9937	−1.2083	7.51781	17.4206	−43.3922	0.98
	1.1	0.0391	−1.6538	9.7126	−1.2556	7.74306	19.6131	−45.7438	0.98
	1.2	0.0758	−2.3863	12.8024	−3.7055	8.57506	21.9906	−50.7156	0.98
	1.3	0.0963	−2.7357	14.0583	−2.7833	10.0549	27.5144	−60.6719	0.98
15	1.0	−0.0086	−3.2486	15.3910	−0.2056	11.5469	20.1288	−63.0312	0.97
	1.1	0.0316	−3.8675	17.5058	−1.2583	12.0959	23.8913	−67.7734	0.97
	1.2	0.0939	−4.9824	21.2692	−3.2639	13.2586	28.6831	−76.0516	0.97
	1.3	0.1458	−6.3380	25.7582	−3.6639	15.7839	36.2119	−91.7422	0.97
20	1.0	−0.2208	−2.9090	14.1746	9.8528	16.3881	18.3413	−82.9594	0.97
	1.1	−0.1624	−4.1290	18.1993	7.8560	17.7729	23.2088	−92.2344	0.97
	1.2	−0.1381	−5.4277	22.0912	7.3833	20.1755	29.525	−106.697	0.97
	1.3	−0.2972	−5.8725	23.3229	13.4111	25.7444	37.4194	−135.216	0.97

Note: Polynomial fitting valid in the range $0.04 \le \theta/\pi \le 0.20$ and $0.1 \le a/t \le 0.5$.

Table 5
Coefficients of polynomial fitting of h_1 factor for mismatched configurations with moderate hardening base material.(n^{BM}=10, E/σ_0=500)

D_e/t	M_y	ζ_0	ζ_1	ζ_2	ζ_3	ζ_4	ζ_5	ζ_6	R^2
10	1.0	−0.3812	−4.9809	51.8813	−45.9639	29.1641	20.1256	−138.4780	0.97
	1.1	−0.6851	−6.6172	73.5477	−63.5583	45.5286	30.5131	−215.3700	0.97
	1.2	−1.3624	−7.0103	110.1650	−96.4583	73.5981	45.1788	−346.8370	0.97
	1.3	−4.8764	4.6989	170.4130	−162.3310	150.007	18.7531	−657.1810	0.95
15	1.0	−0.5809	−14.4687	99.5898	−78.6500	48.1574	22.4263	−221.9170	0.97
	1.1	−0.8654	−22.3262	148.9560	−114.6360	73.8203	36.5731	−341.6190	0.97
	1.2	−1.3634	−37.2248	241.4380	−182.3330	121.0860	61.3306	−562.0660	0.97
	1.3	−2.0702	−47.4144	358.8000	−269.2640	172.1560	70.9581	−806.1580	0.97
20	1.0	−1.5425	−13.6135	105.3680	−58.8944	70.5966	9.4963	−313.7980	0.97
	1.1	−2.8880	−16.1239	138.0650	−54.4806	113.7760	8.4512	−500.5090	0.97
	1.2	−6.5063	−1.6685	157.4170	7.0806	185.3430	−66.4463	−770.0940	0.97
	1.3	−19.7485	42.3067	203.0790	111.8140	429.7880	−370.0160	−1623.900	0.97

Note: Polynomial fitting valid in the range $0.04 \le \theta/\pi \le 0.20$ and $0.1 \le a/t \le 0.5$.

Table 6
Coefficients of polynomial fitting of h_4 factor for mismatched configurations with moderate hardening base material.(n^{BM}=10, E/σ_0=500)

D_e/t	M_y	ζ_0	ζ_1	ζ_2	ζ_3	ζ_4	ζ_5	ζ_6	R^2
10	1.0	−0.2421	−1.2188	22.5160	−16.4778	15.2935	7.6650	−70.9859	0.98
	1.1	−0.4741	−2.1173	36.4013	−26.1861	26.9639	12.8244	−124.3870	0.97
	1.2	−1.1761	−1.7451	58.8323	−41.2583	51.7972	20.7244	−236.4090	0.97
	1.3	−3.5128	3.2251	107.8590	−83.8444	111.7440	10.8881	−486.8810	0.96
15	1.0	−0.3431	−6.2885	47.3874	−32.3778	25.5130	9.3750	−116.3670	0.97
	1.1	−0.6541	−11.6063	81.2763	−54.1972	45.9718	16.0550	−208.5950	0.97
	1.2	−1.6022	−23.7419	157.1230	−102.7060	96.1421	24.6187	−429.1520	0.96
	1.3	−4.4110	−48.9596	318.8440	−209.2690	216.4050	26.7975	−947.0170	0.95
20	1.0	−0.7390	−8.8194	63.3483	−36.5944	38.7199	2.3069	−169.1480	0.97
	1.1	−1.6122	−15.5531	107.3200	−55.4472	74.5795	−0.0425	−321.3190	0.96
	1.2	−4.0639	−27.5266	200.9220	−89.9667	158.8330	−28.2600	−665.7090	0.95
	1.3	−10.4224	−39.3247	362.5890	−118.2080	340.9150	−138.3310	−1384.440	0.95

Note: Polynomial fitting valid in the range $0.04 \le \theta/\pi \le 0.20$ and $0.1 \le a/t \le 0.5$.

Table 7
Coefficients of polynomial fitting of h_1 factor for mismatched configurations with low hardening base material.(n^{BM}=20, E/σ_0=300)

D_e/t	M_y	ζ_0	ζ_1	ζ_2	ζ_3	ζ_4	ζ_5	ζ_6	R^2
10	1.00	−0.1202	3.2180	24.3132	−25.4472	10.4947	−16.5431	−45.3859	0.99
	1.10	−2.7868	34.5116	37.4071	−40.9000	60.5741	−107.224	−236.634	0.99
	1.20	−22.8006	224.7340	44.8333	−89.2444	370.257	−783.679	−1245.94	0.99
	1.25	−22.1854	177.7460	1057.490	−1255.240	701.547	−1440.03	−2522.12	0.99
15	1.00	−0.4984	−2.4027	71.0699	−70.5139	25.0298	−33.8544	−97.6016	0.99
	1.10	−4.8302	16.7598	203.5370	−179.2030	131.11	−197.738	−496.552	0.99
	1.20	−9.6603	−23.8286	1408.700	−1412.020	437.07	−1045.07	−1491.34	0.99
	1.25	−27.2681	183.3610	2126.140	−2253.290	667.728	−2494.71	−1910.60	0.99
20	1.00	−1.0675	−2.2641	83.7755	−65.5778	35.0031	−40.1994	−139.014	0.99
	1.10	−9.8261	3.3686	434.2050	−396.7580	226.9820	−414.929	−756.781	0.99
	1.20	−43.5507	124.2620	1528.140	−1307.790	842.0440	−2048.41	−2548.60	0.99
	1.25	−141.3860	563.3620	1990.850	−1479.120	2494.110	−4263.08	−8372.95	0.99

Note: Polynomial fitting valid in the range $0.04 \le \theta/\pi \le 0.20$ and $0.1 \le a/t \le 0.5$.

contact upon the drum, which is modeled as a rigid surface with diameter of Φ_r=15,000 mm. Hence, beyond this point the reeling method ceases to drive the near-tip forces during crack opening.

Before to address the J integral computation on cracks, the moment-strain relation is studied for this case with different weld strength mismatch levels. A plot of bending moment versus longitudinal strain is shown in Fig. 16a. It is seen that the bending moment decreases as crack depth increases when the axial surface strain is measured from a distance very close (1/68D) to the crack opening (within weld strip) on the top of pipe surface (tension side). From similar plots for other mismacth levels (M_y > 1.15), it was observed that the strain distribution has similar tendency than previous one regarding crack depth but has slightly different magnitude in applied bending moment because of overmatching. This suggests that there is not a significant effect of weld strength mismatch, compared to flaw dimension effects, upon moment-strain relation. The aforementioned results present additional complexities to compute axial strain in pipes subject to bending when axial strain is measured nearby to the crack. The strong variation in moment-strain relation leads to a dissociation between crack-driving force and the applied bending load, whereby the functional dependence given by Eq. (19) does not hold true. Meanwhile, for axial strains measured from a distance of one diameter (1D) from the mid-section of the pipe [25] exhibit a stable moment-strain evolution regardless crack size and mismatch level as shown in Fig. 16b and c. Hence, this definition of strain proves to be convenient way of assessing bending moment for welded pipes irrespective to the neither filler material properties nor crack dimensions.

The maximum J value is obtained when a large portion of pipe makes contact with drum during spooling, as shown in Fig. 17a. This is described in term of load line displacement (LLD, Δ) for a given cracked configuration. In the plot, J follows a rapidly growth in all the way of deformation (expressed by Δ) until it reaches a plateau (Δ~3360 *mm*) that varies according to the crack dimension. The deeper the crack is, the higher the J will be. Because these types of cracks develop higher constraint levels at the crack-tip compared to the shallower one [14,15], thus the peak value of J (J_{reel}) of each configuration depends solely on crack dimension rather than deformation levels.

The predicted value of J (J_{pred}) for each case is derived from the proposed methodology by means of Eq. (1) and its related components given by Eqs. (2) and (6). Meanwhile, the corresponding h_1 factor is computed by a linear interpolation between the given data provided by Tables 3–6 The actual bending moment is obtained from the moment-strain relation presented in Fig. 16. Indeed, the global behavior observed on the pipe subject to bending loads clearly shows its independence from geometry issues such as crack depth, but it is still a function of pipe diameter size and material characteristics [25]. Under pure bending, the axial strain is given by $\varepsilon_z^b = D_e/(2R_b + D_e)$, where D_e is the external diameter and R_b is the bending radius. The maximum longitudinal bending strain ($\varepsilon_{z,max}^b$) is reached by the pipe when the bending radius is comparable to one-half of reel diameter size (R_b=Φ_r/2), which turns out $\varepsilon_{z,max}^b = 0.0225$. Therefore, the maximum applied bending moment can be estimated using Fig. 16b, which enter directly into Eq. (6) to obtain J_p necessary to compute total J.

Fig. 17b shows results obtained from reeling simulations and estimation procedure outlined above, for three different levels of weld strength mismatch with varying crack lengths. The less than 10% prediction error results clearly show the potentiality of such an estimation scheme adopted here to determine J (consequently CTOD) parameter in defective girth welded pipe subject to bending load for all analyzed configurations, which can be considered valid from point of view of engineering.

Table 8
Coefficients of polynomial fitting of h_4 factor for mismatched configurations with low hardening base material.(n^{BM}=20, E/σ_0=300)

D_e/t	M_y	ζ_0	ζ_1	ζ_2	ζ_3	ζ_4	ζ_5	ζ_6	R^2
10	1.00	−0.1942	5.4750	3.0755	0.644444	6.36163	−12.9937	−27.3422	0.99
	1.10	−1.9284	27.7783	26.3790	−19.5167	47.0666	−104.849	−173.677	0.99
	1.20	−8.9528	60.5207	644.2890	−776.464	333.152	−765.682	−1145.99	0.98
	1.25	−38.0719	480.5530	529.0020	−712.761	710.696	−1968.85	−2428.76	0.99
15	1.00	−0.2029	−2.8175	54.7967	−53.0667	16.6502	−27.9431	−62.1	0.99
	1.10	−3.5549	5.5221	225.110	−202.592	108.489	−221.641	−374.687	0.99
	1.20	2.8514	−168.3570	1963.430	−2015.32	359.101	−875.047	−1264.3	0.99
	1.25	−11.8432	−881.4210	8854.450	−8457.04	1815.98	−5745.45	−4809.3	0.99
20	1.00	−1.2451	1.7192	50.6057	−35.5667	30.5571	−41.7388	−113.037	0.98
	1.10	−8.6061	−35.8066	521.9310	−506.3920	258.0590	−369.936	−895.412	0.97
	1.20	−54.8151	−70.2656	2955.300	−2558.690	1224.010	−3078.47	−3380.87	0.98
	1.25	−242.865	1189.070	1706.870	−697.7420	4005.550	−5804.180	−14265.60	0.99

Note: Polynomial fitting valid in the range $0.04 \le \theta/\pi \le 0.20$ and $0.1 \le a/t \le 0.5$.

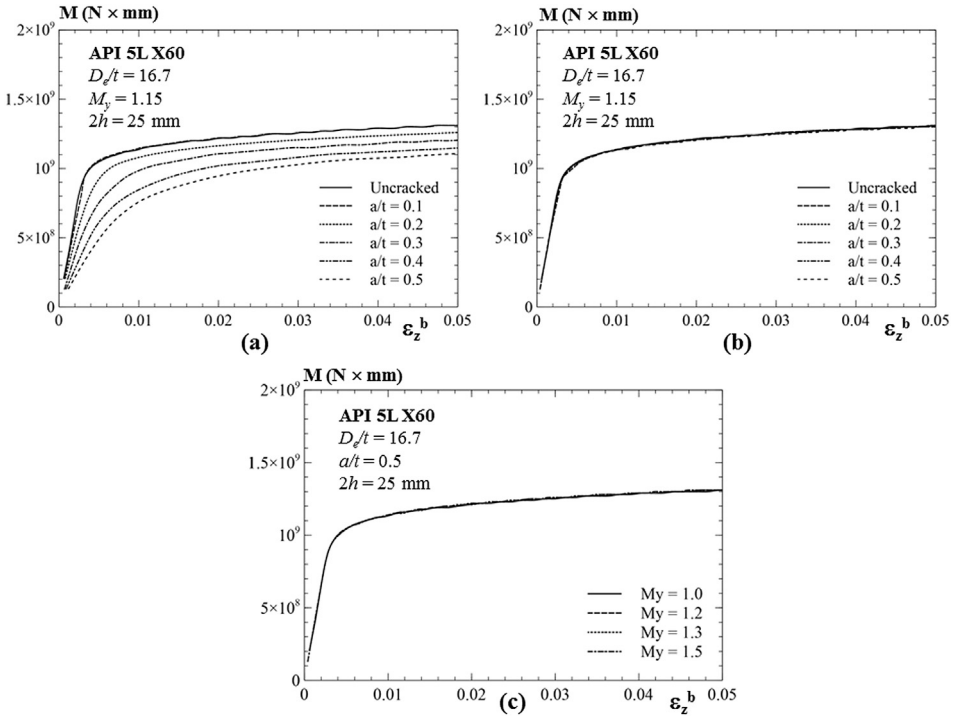

Fig. 16. Moment–Strain relation of API 5L X60 pipeline material for $D_e/t = 16.7$ and $2h = 25$ mm; (a) Longitudinal strain computed from a distance of 1/68 D for $M_y = 1.15$ and various crack depths; (b) Longitudinal strain computed from a distance of 1D for $M_y = 1.15$ and various crack depths; (c) Longitudinal strain computed from a distance of 1D for $a/t = 0.5$ and various M_y.

7. Concluding remarks

The effect of weld strength mismatch on crack driving force of girth weld pipes containing circumferentially surface cracks was analyzed. *J* and CTOD estimation procedure based on fully plastic solutions have proven to be effective in homogeneous conditions for several cracked configuration and also for certain mismatch levels. This engineering approach relies upon univocal relationship between crack-tip stress-strain fields and applied loading that take place in heterogeneous media, on which *h* factors are computed. Further, an applicability analysis provides a window where the proposed methodology is acceptable for field-tip quantities being represented by *h* factors. These results are prove to be valid for a wide range of circumferential crack geometries and overmatch levels in the range of $1.0 \leq M_y \leq 1.3$ for bimetallic configurations having high/moderate strain hardening (n^{BM}=5, 10) material as base plate. Also, for parent metal having low strain hardening (n^{BM}=20) material property, the proposed methodology is also applicable in the range of $1.0 \leq M_y \leq 1.25$. Under those conditions, the coupling between weld strength mismatch and configurational effects can be taken account in a tabular form (given by Tables 3–8) where $h_{1,4}$ factors depend solely on mismatch levels and crack dimensions. A validation procedure is conducted in Section 6 that confirms this fact. FE analysis is performed on an idealized situation on which the girth weld pipe, containing a defect, is being spooled onto a large reel and where the evolution of crack driving force is computed. For all analyzed cases, the predicted results derived from mismatched, fully plastic solutions show good agreement with those values corresponding to numerical simulations displayed on the reeling method. Overall, the estimation errors are below 10% for each cracked specimen and level of overmatch, which corroborates its applicability and robustness in determining

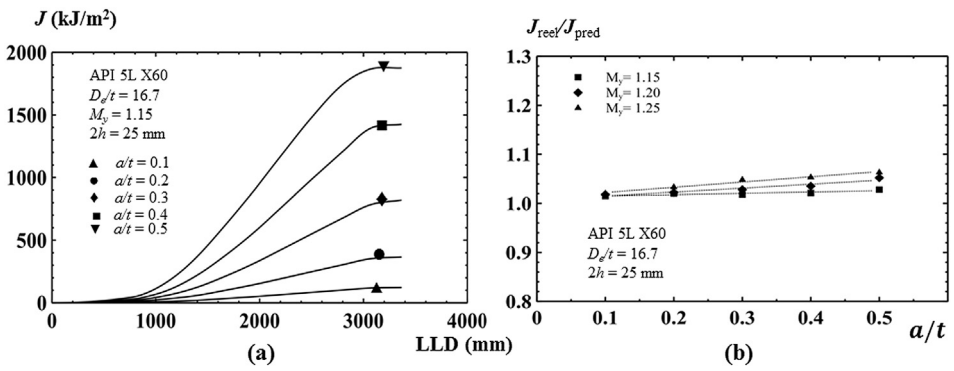

Fig. 17. (a) Evolution of *J* integral versus load-line displacement of cracked pipe for $D_e/t = 16.7$, $M_y = 1.15$, $2h = 25$ mm and various crack depths; (b) Comparison of maximum *J* values between reeling method simulation and estimation scheme based upon fully plastic solutions.

J and CTOD parameters in girth weld pipes with circumferentially oriented flaws subject to bending.

Acknowledgments

This investigation was initially supported by Fundação de Amparo à Pesquisa do Estado de São Paulo (FAPESP) through a graduate scholarship (2008/54208-3) and subsequent was partially supported by MIT Industrial Fracture Consortium provided to the first author (MP). The first author also wants to thank Professor David M. Parks from MIT for his comments on this work.

References

[1] Eiber RJ, Kiefner JF. Failure of pipelines. In: Metals handbook. Failure analysis and prevention. 9th ed., vol. 11. American Society for Metals; 1986. p. 695–706.
[2] American Welding Society. Welding handbook: welding technology. 8th ed., vol. 1. Miami: American Welding Society; 1987.
[3] National Energy Board. Stress corrosion cracking on Canadian oil and gas pipelines. Tech. Rep. MH-2-95. Calgary, CN: National Energy Board; 1996.
[4] Manouchehri S, Howard B, Denniel S. A discussion of the effect of the reeled installation process on pipeline limit states. In: 18th International offshore and polar engineering conference (ISOPE), Vancouver, Canada; 2008.
[5] Wästberg S, Pisarski H, Nyhus B. Guidelines for engineering critical assessments for pipeline installation methods introducing cyclic plastic strain. In: 23rd International Conference on offshore mechanics and arctic engineering (OMAE), Vancouver, Canada; 2004.
[6] American Welding Society. Structural welding code – steel. 2004. AWS D1.1/D1.1M:2004.
[7] American Petroleum Institute. Welding of pipelines and related facilities. API; 2005. 1104.
[8] Det Norske Veritas. Fracture control for pipeline installation methods introducing cyclic plastic strain. 2006. DNV-RP-F108.
[9] Hutchinson JW. Fundamentals of the phenomenological theory of nonlinear fracture mechanics. J Appl Mech 1983;50:1042–51.
[10] Kumar V, German MD, Shih CF. An engineering approach to elastic-plastic fracture analysis. Tech. Rep. EPRI NP-1931. Palo Alto, CA: Electric Power Research Institute; 1981.
[11] Shih CF, Hutchinson JW. Fully plastic solutions and large scale yielding estimates for plane stress crack problems. Trans ASME J Eng Mater Technol - Ser H 1976;98:289–95.
[12] Zahoor A. Ductile fracture handbook. Tech. Rep. EPRI NP-6301–D. Palo Alto, CA: Electric Power Research Institute; 1989.
[13] Chiodo MSG, Ruggieri C. *J* and CTOD estimation procedure for circumferential surface cracks in pipes under bending. Eng Fract Mech 2010;77:415–36.
[14] Anderson TL. Fracture mechanics: fundaments and applications. 3rd ed. CRC Press; 2005.
[15] Dowling NE. Mechanical behavior of materials: engineering methods for deformation, fracture and Fatigue. 2nd ed. New Jersey: Prentice Hall; 1999.
[16] American Petroleum Institute. Fitness-for-service. 2007. API RP-579–1/ASME FFS-1.
[17] Kirk MT, Dodds RH. *J* and CTOD estimation equations for shallow cracks in single edge notch bend specimens. J Test Eval 1993;21:228–38.
[18] Shih CF. Relationship between the *J* -integral and the crack opening displacement for stationary and extending cracks. J Mech Phys Solids 1981;29:305–26.
[19] Gullerud A, Koppenhoefer K, Roy A, RoyChowdhury S, Walters M, Bichon B, et al. WARP3D: dynamic nonlinear fracture analysis of solids using a parallel computers and workstations. Structural research series (SRS) 607. UILU-ENG-95-2012. University of Illinois at Urbana-Champaign; 2004.
[20] Moran B, Shih CF. A general treatment of crack tip contour integrals. Int J Fract 1987;35:295–310.
[21] API specification for 5L line pipe. 42nd ed. American Petroleum Institute API; 2000.
[22] Paredes M, Ruggieri C. Further results in *J* and CTOD estimation procedures for SE(T) fracture specimens. Part II: Weld centerline cracks. Engng Fract Mech 2012;89:24–39.
[23] Brazilian State Oil Company (Petrobras). Tensile tests for an API grade 5L X60 pipeline steel. Private report. 2002 [in Portuguese].
[24] Joch J, Ainsworth RA. Relationships between the *J*-integral and the crack tip opening displacement for stationary cracks in weldments at plastic collapse. Fatigue Fract Engng Mater Struct 1994;17(10):1175–85.
[25] Østby Erling, Jayadevan KR, Thaulow Christian. Fracture response of pipelines subject to large plastic deformation under bending. Int J Press Vessels Pip 2005;82:201–15.